Journal of Inorganic Biochemistry 199 (2019) 110779

Contents lists available at ScienceDirect

Journal of Inorganic Biochemistry

journal homepage: www.elsevier.com/locate/jinorgbio

Pt-Fe ferrocenyl compounds with hydroxyquinoline ligands show selective cytotoxicity on highly proliferative cells

Feriannys Rivas[a], Andrea Medeiros[b,c], Marcelo Comini[b], Leopoldo Suescun[d], Esteban Rodríguez Arce[a], Marta Martins[e], Teresa Pinheiro[f], Fernanda Marques[g], Dinorah Gambino[a,*]

[a] Área Química Inorgánica, Facultad de Química, Universidad de la República, Montevideo, Uruguay
[b] Group Redox Biology of Trypanosomes, Institut Pasteur de Montevideo, Montevideo, Uruguay
[c] Departamento de Bioquímica, Facultad de Medicina, Universidad de la República, Montevideo, Uruguay
[d] Laboratorio de Cristalografía, Química del Estado Sólido y Materiales, Cátedra de Física, DETEMA, Facultad de Química, Universidad de la República, Montevideo, Uruguay
[e] Instituto de Medicina Molecular- João Lobo Antunes, Faculdade de Medicina, Universidade de Lisboa, Lisboa, Portugal
[f] Institute for Bioengineering and Biosciences, Departamento de Engenharia e Ciências Nucleares, Instituto Superior Técnico, Universidade de Lisboa, Bobadela, Portugal
[g] Centro de Ciências e Tecnologias Nucleares, Instituto Superior Técnico, Universidade de Lisboa, Bobadela, Portugal

ARTICLE INFO

Keywords:
Ferrocenyl compounds
Platinum
Hydroxyquinoline derivatives
Trypanosoma brucei
Cancer cells
Anti-proliferative

ABSTRACT

Searching for a more effective chemotherapy for the treatment of Human African trypanosomiasis, the disease caused by the parasite *Trypanosoma brucei*, and cancer, in the current work five new $[Pt^{II}(L)(dppf)](PF_6)$ compounds, with HL = 8-hydroxyquinoline derivatives and dppf = 1,1′-bis(diphenylphosphino)ferrocene, were synthesized and fully characterized. Crystal structures of three compounds were solved by XRD. The compounds displayed fairly good activity against bloodstream *T. brucei,* with IC_{50} values in the submicromolar range (IC_{50}: 0.14–0.93 μM), and good selectivity towards the pathogen (SI: 11 - 48) with respect to mammalian macrophages (cell line J774). Coordination to the {Pt-dppf} moiety led, in most cases, to an enhancement of the activity in respect to the bioactive ligands (11 to 41 fold). Cytotoxicity was assessed against wildtype (A2780) and cisplatin-resistance (A2780cisR) ovarian cancer cell lines. Four $[Pt^{II}(L)(dppf)](PF_6)$ compounds were more active (IC_{50}: 1.2–4.4 μM) than cisplatin (IC_{50}: 26.0 μM) on A2780 cells and showed far superior activity than the reference drug against A2780cisR cells. Platinum levels in A2780 cells showed poor correlation between cellular uptake and the cytotoxic activity. All the complexes interacted with DNA and the most active ones induced reactive oxygen species (ROS) formation which suggested that the mechanism of action for these complexes may be mediated by oxidative stress and interaction with DNA that could act as a potential molecular target for this type of complexes. Some complexes of this series could be considered new hits for the development of prospective agents against trypanosomatid parasites and ovarian cancer.

1. Introduction

Human African trypanosomiasis (HAT) or sleeping sickness is one of the seventeen communicable and poverty-related illnesses considered as neglected diseases by the World Health Organization on account of the scarce attention received from the pharmaceutical industry. This resurgent disease has endemic character in sub-Saharan regions of Africa affecting mainly people living in rural areas. The disease is caused by two subspecies of the protozoa *Trypanosoma brucei* (*T. brucei*), *Trypanosoma brucei gambiense* and *Trypanosoma brucei rhodesiense*, transmitted by the bite of a tsetse fly. Ninety percent of the cases correspond to chronic-like infections caused by *T. b. gambiense* whereas *T. b. rhodesiense* is responsible for the most virulent form of the disease, both being fatal if left untreated. The animal disease, called Nagana and caused by *T. b. brucei* and *T. congolense*, is also threatening since it severely affects stock animals. Five drugs are currently registered for the treatment, namely pentamidine, suramin, melarsoprol, eflornithine and, more recently, fexinidazole. Nifurtimox is also used but in combination with efluornithine. With the exception of fexinidazole, most of these drugs present high toxicity, complex administration, or are susceptible to development of parasite resistance [1–3].

On the other hand, cancer is a generic term for a large group of

* Corresponding author.
E-mail address: dgambino@fq.edu.uy (D. Gambino).

https://doi.org/10.1016/j.jinorgbio.2019.110779
Received 13 May 2019; Received in revised form 12 July 2019; Accepted 14 July 2019
Available online 16 July 2019
0162-0134/

diseases characterized by the growth of abnormal cells beyond their usual boundaries that can then invade adjoining parts of the body and/or spread to other organs. It is a main public health concern worldwide being the second leading cause of death globally. It was estimated to account for 9.6 million deaths in 2018 [4]. Treatment of cancer using specific anti-cancer drugs repeatedly failed. For example, in ovarian cancer, a gynecologic cancer often associated with high mortality rates, no effective drugs are available for the advanced stage of the disease. Cisplatin, the classical platinum-based drug, has become the standard of care for advanced ovarian cancer. However, the problems of drug resistance and the severe side effects that entail the treatment decrease their efficacy and contribute to debilitation of the patients. To overcome these constraints research on the development of novel platinum-based drugs with a better outcome must be pursued [5].

The modern establishment of the Medicinal Inorganic Chemistry field, determined by the discovery of the cytotoxic activity of cisplatin, has led to a pushing research area looking for new metal-based chemotherapeutics with better biological profiles[6].

Although most efforts have been done in the development of antitumoral compounds, the development of metal-based drugs has also shown to be a promising approach in the search for new chemotherapeutics for the treatment of parasitic diseases. Prospective metal-based drugs against highly prevalent parasitic illnesses have been identified by different groups in the last years [7–15].

Several ferrocenyl derivatives have shown promising antiparasitic or antitumoral activities. In particular, the “sandwich type” ferrocene moiety has shown high potential in the development of novel organometallic drugs. A good example of this are the antitumoral ferrocifen and the antimalarial ferroquine, that have entered the phase of clinical trials. Ferrocene derivatives are in general easy to prepare, and stable in air and in solution. They usually show low cytotoxicity and adequate lipophilicity that favors compound's penetration across cell membranes. In addition, the generation of reactive oxygen species (ROS) shown by ferrocene derivatives like ferroquine could have therapeutic significance, since trypanosomatid parasites are particularly sensitive to radical species [16–19]. In fact, several ferrocenyl derivatives have shown promising antitrypanosomal activities [9,20–22].

In this context, the research by our group on this topic has been focused on the rational design of new organometallic prospective metal-based drugs for the treatment of diseases caused by trypanosomatid parasites. The strategy has mainly involved incorporating bioactive ligands, pharmacologically active metals and selected organometallic *cores* in the same molecule [9].

Our current interest in both, trypanosomiases and cancer, is due to the urgent need of new drugs for the treatment of both types of diseases but also to some metabolic similarities observed between both highly proliferative cells, trypanosomatid parasites and tumor cells. These resemblances could lead to a correlation between antiparasitic and antitumor activities of the compounds. In fact, several antitumoral drugs also show significant antiparasitic activity and *vice versa* [23,24].

Among the series of compounds previously developed by us, a privileged series of organometallic compounds, including fourteen Pd and Pt 1,1′-bis(diphenylphosphino)ferrocene (dppf) derivatives with three different families of bidentate bioactive ligands, showed interesting activity against *T. brucei* and/or *T. cruzi*. Instead of designing organic compounds with a ferrocenyl moiety, the ferrocene scaffold was included in the compounds as the organometallic co-ligand dppf [25–29].

In the current work, searching for new compounds including this {M-dppf} moiety, five new $[Pt^{II}(L)(dppf)](PF_6)$ compounds, with HL = 8-hydroxyquinoline derivatives, were synthesized and fully characterized in the solid state and in solution (Fig. 1). The biological activity of the compounds against the bloodstream form of *T. b. brucei* and murine macrophages (cell line J774) was evaluated to determine their antitrypanosomal potency and selectivity towards the parasite. In addition, their antitumoral activity against ovarian cancer cell lines sensitive (A2780) and resistant (A2780cisR) to cisplatin was assessed. To get insight into the potential mechanism of action of the new compounds, the generation of ROS in A2780 cancer cells and the interaction with DNA were explored.

2. Materials and methods

2.1. Materials

All common laboratory chemicals were purchased from commercial sources and used without further purification. 8-hydroxyquinoline and derivatives were purchased from Sigma Aldrich. 8-hydroxyquinoline, 5-nitro-8-quinolinol and 5-chloro-7-iodo-8-quinolinol sodium salts (NaL1, NaL2 and NaL3) were prepared through a literature procedure [30]. $[PtCl_2(dppf)]\cdot CHCl_3$ precursor was synthesized according to a previously reported procedure by heating for 30 min an equimolar mixture of $[PtCl_2(dmso)_2]$ and dppf in $CHCl_3$ [31].

2.2. Synthesis of $[Pt^{II}(L)(dppf)](PF_6)$ compounds, HL = HL1-HL5

The $[Pt(L)(dppf)](PF_6)$ compounds were synthesized by the following procedure: 50 mg of precursor $[PtCl_2(dppf)]\cdot CHCl_3$ (0.053 mmol) were dissolved in 10 mL of methanol. For $[Pt(L)(dppf)](PF_6)$ compounds, where HL = HL1-HL3, an equimolar amount of ligand sodium salt dissolved in 5 mL of methanol was added. For $[Pt(L)(dppf)](PF_6)$ compounds, where HL = HL4 and HL5, an equimolar amount of ligand dissolved in methanol including triethylamine was added. The mixture was kept under reflux for 5 h for $[Pt(L2)(dppf)](PF_6)$ compound. The rest of the compounds were kept under stirring for 24 h. The solution was evaporated up to 5 mL and centrifugated. $NaPF_6$ in 200% excess (0.159 mmol) dissolved in a minimal volume of methanol was added. The solution was kept in refrigerator during 24 h. The compounds were isolated by centrifugation as orange-yellow solids. The compounds were recrystallized from a dichloromethane solution of the compounds by diffusion with hexane.

[Pt(L1)(dppf)](PF$_6$), Pt-dppf-L1. Yield: 25 mg, 46%. Anal. calc. for $C_{43}H_{34}F_6FeNOP_3Pt$: C, 49.73; H, 3.30; N, 1.35. Found: C, 50.07; H, 3.29; N, 1.37.

[Pt(L2)(dppf)](PF$_6$), Pt-dppf-L2. Yield: 19 mg, 32%. Anal. calc. for $C_{43}H_{33}F_6FeN_2O_3P_3Pt$: C, 47.66; H, 3.07; N, 2.59. Found: C, 47.27; H, 3.36; N, 2.49.

[Pt(L3)(dppf)](PF$_6$), Pt-dppf-L3. Yield: 31 mg, 52%. Anal. calc. for $C_{43}H_{32}Cl_2F_6FeNOP_3Pt$: C, 46.63; H, 2.91; N, 1.26. Found: C, 46.39; H, 2.68; N, 1.20.

[Pt(L4)(dppf)](PF$_6$), Pt-dppf-L4. Yield: 38 mg, 60%. Anal. calc. for $C_{43}H_{32}ClF_6FeINOP_3Pt$: C, 43.09; H, 2.67; N, 1.17. Found: C, 42.87; H, 2.73; N, 1.21.

[Pt(L5)(dppf)](PF$_6$), Pt-dppf-L5. Yield: 48 mg, 63%. Anal. calc. for $C_{43}H_{32}F_6FeI_2NOP_3Pt$: C, 40.02; H, 2.50; N, 1.09. Found: C, 39.65; H, 2.65; N, 1.06.

2.3. Physicochemical characterization

C and H analyses were carried out with a Thermo Scientific Flash 2000 elemental analyzer. Conductimetric measurements were done over time (7 days) at 25 °C in 10^{-3} M DMSO solutions using a Conductivity Meter 4310 Jenway to determine the type of electrolyte and to assess the stability of the complexes in such medium [32]. The FTIR spectra (4000–400 cm^{-1}) were measured as KBr pellets with a Shimadzu IRPrestige-21 instrument. ^1H NMR spectra were recorded in DMSO-d_6 at 30 °C on a Bruker DPX-400 instrument at 400 MHz. Homonuclear correlation (COSY) experiments were carried out with the same instrument. Tetramethylsilane was used as the internal standard. Chemical shifts are reported in ppm.

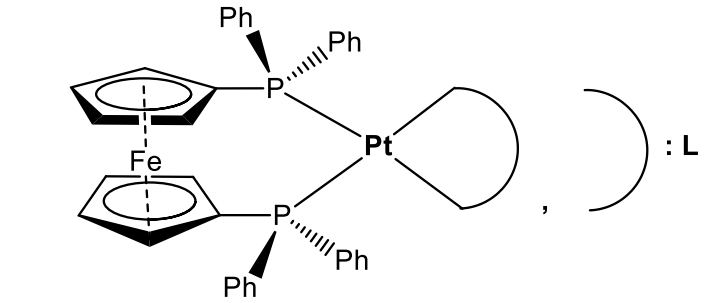

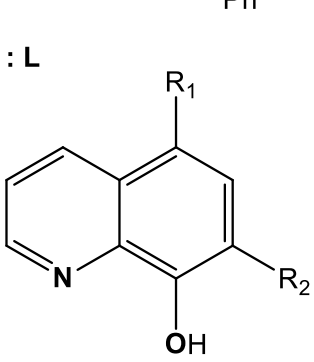

	R_1	R_2	
8-hydroxyquinoline	H	H	**HL1**
5-nitro-8-quinolinol	NO_2	H	**HL2**
5,7-dichloro-8-quinolinol	Cl	Cl	**HL3**
5-chloro-7-iodo-8-quinolinol	Cl	I	**HL4**
5,7-diiodo-8-quinolinol	I	I	**HL5**

Fig. 1. Structures of the 8-hydroxyquinoline derivatives HL and of the new heterobimetallic 1,1′-bis(dipheny1phosphino) ferrocene (dppf) complexes [Pt^{II}(L)(dppf)](PF_6).

2.4. X-ray diffraction study of [Pt(L)(dppf)](PF_6) compounds, where HL = HL1, HL2 and HL3

Single crystals suitable for X-ray diffraction studies of three compounds, [Pt^{II}(L1)(dppf)](PF_6), [Pt^{II}(L2)(dppf)](PF_6) and [Pt^{II}(L3)(dppf)](PF_6), were obtained by slow diffusion of hexane into dichloromethane solutions of the complexes. Measurements were performed on a Bruker D8 Venture diffractometer with multilayer mirror monochromated MoKα (λ = 0,71073 Å) radiation for Pt-dppf-L1 and Pt-dppf-L3 compounds and monochromated CuKα (λ = 1.54178 Å) radiation for Pt-dppf-L2 compound. X-ray diffraction intensities were collected with APEX 2 v2014.5-0 (Bruker AXS) and integrated with APEX3 v2017.3-0 (Bruker AXS). These intensities were scaled and the data were corrected empirically for absorption (employing the multi-scan method) with the SADABS v2016/2 (SADABS-2016/2 - Bruker AXS) program [33]. The structures were solved by hybrid methods with the SHELXT and the molecular model developed by alternated cycles of Fourier methods and full-matrix least-squares refinement with Olex2 for Pt-dppf-L1 and SHELXL-2017 running under SHElXle for Pt-dppf-L2 and Pt-dppf-L3 complexes [34–36]. The hydrogen atoms were positioned on stereo-chemical basis and refined with the riding model. Crystal data, data collection procedure, structure determination methods and refinement results are summarized in Table 1.

2.5. Biological studies

2.5.1. Viability assays for bloodstream Trypanosoma b. brucei

The anti-trypanosomal activity of the compounds was evaluated against bloodstream *T. b. brucei* (monomorphic strain 427, cell line 449-hGrxroGFP2) [37]. The parasites were cultivated aerobically in Iscove's Modified Dulbecco's Medium (HMI-9) medium supplemented with 10% (v/v) fetal bovine serum (FBS), 10 U/mL penicillin, 10 µg/mL streptomycin, 0.2 µg/mL phleomycin and 5 mg/mL hygromycin, inside a humidified incubator at 37 °C and 5% CO_2. Stock solutions (25 mM) in DMSO were prepared for each compound. All assays were started with parasites from an exponential-phase culture and compounds were added at different concentrations to estimate their IC_{50} values. The reference drug Nifurtimox was assayed at its IC_{50} value of 15 µM whereas the final concentration of DMSO in all conditions tested was ≤1% (v/v). Cytotoxicity was assayed from triplicate biological samples, as previously described, using propidium iodide (PI, final concentration 2 µg/mL) as exclusion dye and BD Accuri C6 (BD Biosciences) or CyAn™ADP (DakoCytomation) flow cytometers [38]. IC_{50} values were obtained from dose-response curves, fitted to a sigmoidal Boltzmann equation (errors calculated using errors' propagation) or extrapolated from non-linear fitting plots. The errors are expressed as one standard deviation (S.D., estimated as σ^{n-1}).

2.5.2. Cytotoxicity assays on murine macrophages

Mouse macrophages from the cell line J774 (ATCC® TIB-67™) were cultivated in a humidified 5% CO_2/95% air atmosphere at 37 °C in Dulbecco's Modified Eagle medium (DMEM) supplemented with 10% (v/v) FBS, 10 U/mL penicillin and 10 µg/mL streptomycin. The experimental protocol for the determination of IC_{50} values was previously described [39], except that 200 µL of a cell suspension at 6×10^4 cells/mL was added per well in a 96-well culture plate. The cytotoxicity of the compounds was evaluated at five different concentrations (0.01–100 µM) in triplicates and using the WST-1 reagent (Roche) (2-(4-Iodophenyl)-3-(4-nitrophenyl)-5-(2,4-disulfophenyl)-2H-tetrazolium sodium salt). A control included cells treated with DMSO 1% (v/v). Absorbance at 450 nm, corresponding to the formazan dye produced by metabolically active cells, was measured with an EL 800 microplate reader. IC_{50} values were obtained from drug-response curves as described above for the *T. brucei* assay and the associated errors are expressed as S.D.

2.5.3. Cytotoxicity assays on ovarian cancer cells and normal fibroblasts

A2780 (ECACC, 93112519) and A2780cisR (ECACC, 93112517) ovarian cells (Sigma-Aldrich) and V79 (ATCC CCL-93) non-cancer lung Chinese hamster fibroblasts were grown in Roswell Park Memorial Institute medium (RPMI, Gibco) supplemented with 10% FBS (Gibco) in a humidified 5% CO_2/95% air atmosphere at 37 °C. For the assays the

Table 1
Crystal data and structure refinement results for [Pt(L)(dppf)](PF_6) compounds, where HL = HL1, HL2 and HL3.

	Pt-dppf-L1	Pt-dppf-L2	Pt-dppf-L3
Empirical Empirical formula	$C_{43}H_{34}F_6FeNOP_3Pt$	$C_{45}H_{37}Cl_4F_6FeN_2O_3P_3Pt$	$C_{43}H_{32}Cl_2F_6FeNOP_3Pt$
Formula weight	1038.59	1253.41	1107.44
Temperature (K)	298(2)	296	273
Wavelength (Å)	MoKα (λ = 0.71073)	CuKα (λ = 1.54178)	MoKα (λ = 0.71073)
Crystal system	Monoclinic	Triclinic	Monoclinic
Space group	$P2_1/c$	P-1	$P2_1/c$
Unit cell dimensions			
a (Å)	10.6410 (4)	10.379 (1)	12.013 (2)
b (Å)	27.265 (1)	12.995 (1)	36.915 (7)
c (Å)	16.1928 (7)	18.123 (2)	9.755 (2)
β (°)/α, β, γ (°)	101.470 (2)	102.163 (8); 92.428 (8); 94.445 (8)	111.00 (3)
Volume ($Å^3$)	4604.1 (3)	2377.9 (5)	4038.7 (2)
Z; density (calculated, g cm^{-1})	4; 1.4982	2; 1.751	4; 1.821
Absorption coefficient (mm^{-1})	3.509	11.465	4.135
F (000)	2037.2	1232.0	2168.0
Crystal shape/color	Prism/yellow	Prism/orange	Prism/orange
Size (mm^3)	0.264 × 0.13 × 0.11	0.284 × 0.172 × 0.115	0.405 × 0.128 × 0.124
ϑ (°) range for data collection	5.8 to 52.3	3.5 to 67.7	2.8 to 30.1
Index ranges	$-13 \le h \le 13$, $-33 \le k \le 33$, $-20 \le l \le 20$	$-12 \le h \le 12$, $-15 \le k \le 15$, $-21 \le l \le 21$	$0 \le h \le 16$, $-51 \le k \le 0$, $-12 \le l \le 11$
Collected reflections	124,124	30,829	9322
Independent reflections	9154	8556	9322
Observed reflections [$I > 2\sigma(I)$]	7825	6040	6942
Completeness (%)	99.7	99.3	78.5
Absorption correction	Multi-scan	Multi-scan	Multi-scan
Máx. and min. transmission	0.7453 and 0.5791	0.3840 and 0.2169	0.4721 and 0.7460
Refinement method		Full-matrix least-squares on F^2	
Data/restrains/parameters	9154/36/504	8556/189/586	9322/324/558
Goodness-of-fit on F^2	1.064	1.046	1.049
Final R indices[a] [I > 2σ(I)]	$R_1 = 0.0296$; $wR_2 = 0.0648$	$R_1 = 0.0541$; $wR_2 = 0.1333$	$R_1 = 0.0568$; $wR_2 = 0.1478$
R índices (all data)	$R_1 = 0.0387$; $wR_2 = 0.0696$	$R_1 = 0.0878$; $wR_2 = 0.1579$	$R_1 = 0.0814$; $wR_2 = 0.1606$
Largest diff. peak and hole (e.$Å^{-3}$)	1.32 and −0.83	0.65 and −0.99	0.92 and −1.58

[a] $R_1 = \Sigma||F_o|-|F_c||/\Sigma|F_o|$, $wR_2 = [\Sigma w(|F_o|^2-|F_c|^2)^2/\Sigma w(|F_o|^2)^2]^{1/2}$

medium was removed, the cells were washed with PBS and harvested with trypsin-EDTA (Gibco) and then seeded in 96 well plates. Cytotoxicity was assessed by the colorimetric MTT (3-(4,5-dimethylthiazolyl-2)-2,5-diphenyltetrazolium bromide) assay. Briefly, cells (2×10^4 cells/well) were incubated with the compounds previously solubilized in DMSO and then in medium at serial dilutions in the range 0.1–100 μM for 24 h at 37 °C. At the end of the incubation period, the compounds were discarded and the cells were incubated with 0.2 mL of MTT solution (0.5 mg/mL PBS). After 3 h at 37 °C, the solution was removed and the resulting formazan crystals were dissolved in 0.2 mL of DMSO. The cellular viability was evaluated by measuring the absorbance in each well at 570 nm using a plate spectrophotometer (Power Wave Xs, Bio-Tek). Each assay was repeated at least twice and each concentration was tested in at least six replicates. The IC_{50} values were calculated from dose-response curves using the GraphPad Prism software (version 5.0).

2.6. Lipophilicity studies

Reversed-phase TLC experiments were performed on precoated TLC plates SIL RP-18 W/UV_{254} and eluted with MeOH:DMF:H2O (65:5:30 v/v/v). Stock solutions were prepared in pure dichloromethane (Aldrich) prior to use. The plates were developed in a closed chromatographic tank, dried and the spots were detected under UV light. The Rf values were averaged from two to three determinations, and converted to R_M *via* the relationship: $R_M = \log_{10}[(1/R_f) - 1]$ [40,41].

2.7. Insight into the mechanism of action

2.7.1. DNA interaction by fluorescence studies

Experiments for competitive binding to calf thymus DNA (ctDNA, SIGMA, Type I, No. D-1501) with ethidium bromide (EB, SIGMA) were carried out in 10 mM Tris-HCl buffer at pH 7.4. Millipore® water was used for the preparation of all aqueous solutions. Fluorescence measurements were carried out on individually prepared samples to ensure the same pre-incubation time for all samples in each assay. Due to the low solubility of the complexes in aqueous media, DMSO was used to prepare concentrated stock solutions followed by appropriate dilution to obtain the targeted concentration and the same content of DMSO (5% v/v) in the final samples. DNA stock solutions were prepared by hydrating ctDNA in Tris-HCl buffer (1 mg/mL, ~2 mM nuc^{-1}) by gently stirring the solution during 2–3 days. This solution was stored at 4 °C (in the fridge) in-between measurements. The concentration of the stock solution was determined by UV spectrophotometry using the molar absorption coefficient ε (260 nm) = 6600 M^{-1} cm^{-1} nuc^{-1} [42]. An EB 5 mM solution was prepared in Tris-HCl buffer. ctDNA was pre-incubated with EB at 4 °C for 24 h. Samples were prepared with a total concentration of DNA and of EB of 20 μM nuc^{-1} and 10 μM, respectively, varying the total complex concentration from 5 to 110 μM. They were incubated at 37 °C for 30 min. Samples with complex alone, samples with complex and DNA and samples with complex and EB but no DNA were used as blanks. Fluorescence spectra were recorded from 540 nm to 630 nm at an excitation wavelength of 510 nm on an Infinite M200 PRO TECAN plate spectrofluorimeter.

2.7.2. Intracelullar ROS levels in A2780 cells

Intracellular ROS levels in A2780 cells were measured by using the fluorescent probe dihydro-2'7'dichlorofluorescein diacetate (H_2DCFDA). Cells (2×10^4/well) were seeded in 96-well plates and left to grow overnight. Then, medium was replaced with a solution of 10 μM H_2DCFDA in colorless Dulbecco's Modified Eagle Medium/Nutrient Mixture F-12 (DMEM/F12) and cells were incubated at 37 °C for 30 min. This solution was then removed, and cells were incubated with complexes at 10 μM and 50 μM for 1 and 3 h. Dichlorofluorescein

(DCF) fluorescence was measured using an Infinite 200 Plate Reader (Tecan) at 492 nm excitation and 517 nm emission. Each experiment was repeated twice and each concentration was tested with at least three replicates. Results (mean ± SD) were expressed as relative luminescent units (RLU).

2.8. ICP-MS analysis

Platinum was determined by Inductively coupled plasma mass spectrometry (ICP-MS) in A2780 cells (~10^6 cells), which were incubated with the compounds at concentrations equivalent to their IC_{50} values for 24 h at 37 °C. Cell pellets were obtained by centrifugation after washing the cells with PBS to remove the remaining medium. The freeze-dried pellets were acid digested in HNO_3 (suprapur, Merck, Germany) combining ultrasound (60 min at 60 °C) and microwave (350 W, 15 s) radiation. The resulting solution was appropriately diluted for Pt analysis using a quadrupole ICP-MS (ELAN DRCe, PerkinElmer-SCIEX, USA) equipped with a Peltier quartz cyclonic spray chamber and a concentric Meinhard nebulizer. Standards (Calibration Standard 4, PerkinElmer Inc., USA), samples and blanks were prepared using H_2O (18 MΩ·cm, Milli-Q Element®) acidified at 5% v/v HNO_3 (suprapur, Merck, Germany) and doped with 10 μgL^{-1} Yttrium (Y) (AAS Specpure®, Alpha Aesar). Data were collected, processed and analyzed with ELAN 3.4 software. Method validation and uncertainty estimation were described elsewhere [43,44].

3. Results and discussion

Five new Pt(II) organometallic heterobimetallic compounds with 8-hydroxyquinoline derivatives [Pt^{II}(L)(dppf)](PF_6), where HL = HL1-HL5 (Fig. 1), were obtained with high purities and good yields and they were exhaustively characterized in the solid state and in solution. Elemental analyses agreed with the proposed formula.

3.1. Characterization in the solid state

3.1.1. IR spectroscopic characterization

Most relevant IR vibration bands of the five complexes were tentatively assigned based on previous assignments performed on compounds containing 8-hydroxyquinoline derivatives as ligands or dppf (Tables S1–S5) [45–51]. The infrared spectra of the 8-hydroxyquinoline derivatives HL1 – HL5 show three main vibration bands: ν(O—H), ν(C=N) and ν(C—O). A strong ν(C=N) band around 1500–1480 cm^{-1} is observed. After complexation this band is slightly displaced to lower energies, as previously reported for related complexes [52,53]. This fact could be related with the donor character of the nitrogen atom, decreased by the presence of electronegative groups in the ring [54]. On the other hand, the band assigned to the ν(C—O) vibration is displaced to higher energies after complex formation, indicating coordination through the phenolate oxygen atom. This behavior has been observed in other complexes [45,48,49,52,53,55]. In the case of HL2 and its new Pt (II) complex, strong bands around 1500 and 1280 cm^{-1} were assigned to $\nu(N-O)_{as}$ and $\nu(N-O)_s$ vibrations, respectively. These bands were also displaced after complexation. As expected, the medium intensity ν(O—H) vibration band around 3200–3400 cm^{-1} is absent in the five complexes due to deprotonation of the ligands. The typical five signals pattern of the dppf moiety and both strong signals of the hexafluorophosphate anion were also identified in the spectra of the five new complexes [51,56].

3.1.2. Crystal structure of [Pt^{II}(L)(dppf)](PF_6) (HL = HL1, HL2 and HL3)

Single crystals of [Pt(L)(dppf)](PF_6), where HL = HL1, HL2 and HL3, suitable for X-ray diffraction studies were obtained by slow diffusion of hexane into a dichloromethane solution of the compounds. Figs. 2, S1 and S2 show the ORTEP drawings of the L1, L2 and L3 [Pt(L)(dppf)](PF_6) compounds, respectively. Intra-molecular bond distances and angles around the metal center of the three complexes are given in Table 2.

Compounds [Pt(L1)(dppf)](PF_6) and [Pt(L3)(dppf)](PF_6) crystallize in the monoclinic $P2_1/c$ space group, while [Pt(L2)(dppf)](PF_6) crystallize in the triclinic P-1 space group. The central metal ions are in a nearly planar trapezoidal environment, *cis* coordinated to a 8-hydroxyquinoline moiety acting as a bidentate ligand through the oxygen and nitrogen atoms, and to the 1,1′-bis (diphenylphosphino) ferrocene molecule acting as a bidentate ligand through its phosphorous atoms. [Pt(L)(dppf)](PF_6) structures show Pt—O and Pt—N distances in the same range observed in other complexes with these ligands (Table 2) [48,50,57-59].

In the three complexes, the dppf ligand showed the expected Archimidean pentagonal anti-prism conformation for the coordination around the iron in the ferrocene fragment, with the *Cp* rings staggered to each other. The Fe—C distances range from 2.007 to 2.076 Å in the Pt-dppf-L1 complex, 1.974 to 2.064 Å in the Pt-dppf-L2 complex and 2.007 to 2.086 Å in the Pt-dppf-L3 complex. The Pt—P distances lie also in the normal ranges observed in others complexes with the bidentate ligand dppf (Table 2) [25,26]. Two different positions of the anion hexafluorophosphate of Pt-dppf-L3 complex were found in a ratio 7:3. This positional disorder was refined using geometry (SADI, SAME) and Uij restraints (SIMU, RIGU) implemented in SHELXL [34]. Crystallographic structural data have been deposited at the Cambridge Crystallographic Data Centre (CCDC). Any request to the CCDC for this material should quote the full literature citation and the reference number CCDC 1914040 for [Pt^{II}(L1)(dppf)](PF_6), CCDC 1913864 for [Pt^{II}(L2)(dppf)](PF_6) and CCDC 1913863 for [Pt^{II}(L3)(dppf)](PF_6).

3.2. Characterization in solution

Conductivity measurements of DMSO 10^{-3} M solutions led to molar conductivity values (≈25 Scm^2/mol) in the range reported for 1:1 electrolytes, in agreement with the proposed structures [32]. No conductivity changes were observed during at least 7 days at 25 °C. In addition, new peaks due to release of free ligands were not detected in ^1H NMR spectra followed with time. Both results suggest that the complexes are stable in DMSO solution.

3.2.1. NMR results

^1H NMR spectra were recorded to completely characterize the obtained complexes in DMSO-d_6 solution. Two-dimensional COSY NMR experiments aided in the assignment of the spectra. Results of the experiments for the ligands and the complexes are shown in Table 3.

All the complexes showed a similar pattern of signals corresponding to the protons of the 8-hydroxyquinoline moiety and the dppf ligand. Integrations and multiplicities of the signals are in accordance with the obtained stoichiometry of the complexes. In the region of 6–10 ppm signals of the protons of the L ligands and of the phosphine substituents of dppf were observed and assigned. Because of metal coordination, the signals of the protons of the hydroxyquinoline moiety shifted. The ^1H NMR spectra of all free ligands show a doublet (or doublet of doublets) at lowest field. This signal was assigned to proton 2 (see Table 3) in the case of HL1 and all disubstituted derivatives [60]. Due to the proximity of this proton to the metal center, this signal shifts significantly to lower fields after coordination. This behavior has been observed in other complexes with hydroxyquinoline ligands acting in a bidentate way [60-62]. For the monosubstituted derivative (HL2), the doublet at lowest field was assigned to proton 4, highly shifted to lower fields due to the inductive effect of the attracting nitro group. This same signal shifted to higher field in the case of Pt-dppf-L2 complex. In the spectra of the free unsubstituted or monosubstituted ligands HL1 and HL2, the signal located around 6 ppm corresponds to proton 7, the most shielded due to its proximity to the oxygen atom, charge density donor [60-61]. This signal if shifted to higher fields after complexation. As expected, this signal does not appear in the spectra of the compounds with

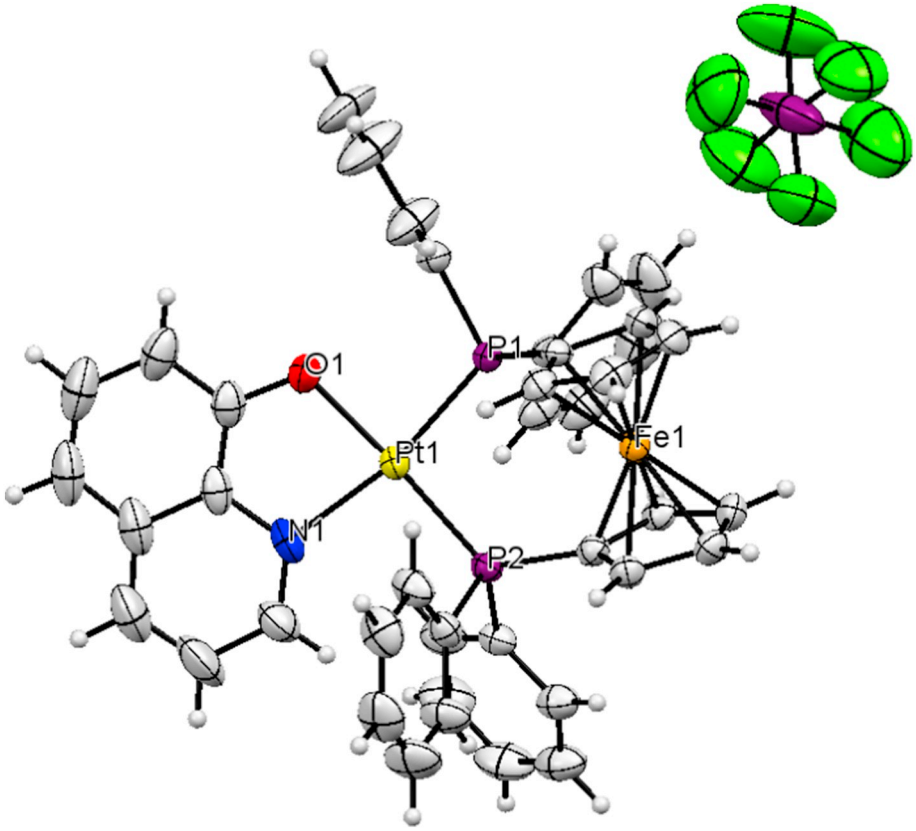

Fig. 2. Drawing of the platinum(II) complex in the [Pt(L1)(dppf)](PF$_6$) solid showing the atomic displacement ellipsoids at the 50% probability level.

Table 2
Bond lengths (Å) and angles (°) around the metal center in [Pt(L)(dppf)](PF$_6$) complexes (HL = HL1, HL2, HL3).

	Pt-dppf-L1	Pt-dppf-L2	Pt-dppf-L3
Bond lengths (Å)			
Pt-O1	2.033 (3)	2.036 (4)	2.062 (5)
Pt-N1	2.122 (3)	2.127 (6)	2.109 (8)
Pt-P1	2.2580 (9)	2.260 (1)	2.261 (3)
Pt-P2	2.2572 (9)	2.263 (1)	2.266 (2)
Bond angles (°)			
O1-Pt-P1	86.48 (8)	87.2 (2)	88.0 (2)
P2-Pt-P1	97.48 (3)	95.91 (6)	97.0 (8)
P2-Pt-O1	173.11 (9)	176.9 (1)	174.8 (2)
N1-Pt-P1	167.3 (1)	166.7 (1)	168.4 (2)
N1-Pt-O1	80.8 (1)	79.6 (2)	80.4 (3)
N1-Pt-P2	95.2 (1)	97.3 (2)	94.6 (2)

hydroxyquinolines disubstituted in positions 5 and 7.

In the spectrum of Pt-dppf-L1, the signal associated with proton 6 was assigned through COSY experiments, given its coupling with proton 7. In the spectra of the compounds with disubstituted hydroxyquinolines, this signal is shown as a singlet, which varies greatly its displacement from one complex to another depending on the substituents of the phenolic ring. Multiplets corresponding to the protons of the PPh_2 moieties of the dppf ligand were also observed. The PPh_2 moieties of free dppf lead to two singlets [7.22 (s) (8) and 7.33 (s) (12)]. For the five Pt-dppf complexes these signals split into multiplets integrating globally for 20 protons and shift to higher chemical displacements.

In the region of 3.4–5.4 ppm signals of the protons of the *Cp* rings of the dppf ligand were observed. For the free dppf, two proton signals (singlets, four proton integration) at 3.94 and 4.27 ppm were observed. These signals have been assigned to equivalent Ha-Hb and Hc-Hd protons of both *Cp* rings that are coplanar to each other and appear like an average eclipsed conformation at room temperature (Table 3) [63]. In the spectra of all five Pt compounds a four signals pattern was observed, indicating lost of fluxionality of the {Pt-dppf} moiety after complexation [64,65]. This behavior has been previously observed for other M-dppf complexes with bidentate ligands [25,26].

3.3. Biological results

3.3.1. Anti - T. brucei activity and selectivity towards the parasite

The antitrypanosomal activity of the different Pt-ferrocenyl derivatives and the corresponding ligands and dppf was evaluated against the bloodstream form of *T. brucei* (Table 4).

All the free ligands showed antiparasitic activity, mostly in the micromolar range. IC_{50} values of free ligands were lower than that of the reference antitrypanosomal drug Nifurtimox (IC_{50} = 15 μM, same technique). The free coligand dppf lacked antiparasitic activity when tested up to 10 μM (note: higher concentrations could not be tested due to the poor solubility of the compound in the parasite culture medium). With exception of HL2, whose activity remained almost unchanged, the complexation of the bioactive ligands to the {Pt-dppf} moiety increased significantly their anti-trypanosomal activity, exhibiting IC_{50} values in the submicromolar range in all cases. The highest effect was observed for the HL1 ligand, which increased its activity by > 41-fold when coordinated. Similarly, the activity increased between 11- to 17-fold for HL3-HL5 when coordinated to the {Pt-dppf} moiety. Worth noting, all complexes proved to be one (16-fold) to two-orders (107-fold) of magnitude more potent than Nifurtimox.

In order to get insight into the biological selectivity of the five metal compounds, their cytotoxicity against macrophages (J774 murine cell line) was tested (Table 4). Among the free ligands, dppf (IC_{50} 45 μM), HL4 (IC_{50} 39 μM) and HL5 (IC_{50} 49 μM) present a quite similar toxicity towards macrophages. The most cytotoxic ligand was HL1 (IC_{50}

Table 3
^{1}H NMR chemical shift values (δ, in ppm) of the ligands and the complexes in DMSO-d_6.

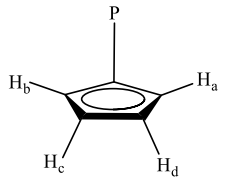

***Cp* ring (dppf)**

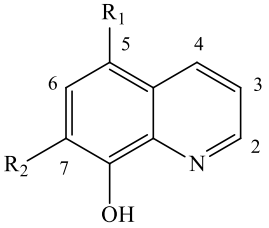

8-hydroxyquinoline

HL1 R_1:H, R_2:H
HL2 R_1:NO_2 , R_2: H
HL3 R_1:Cl , R_2:Cl
HL4 R_1:Cl , R_2:I
HL5 R_1:I , R_2:I

H	δ_H (multiplicity)(integration)													
	HL1	Pt-dppf-L1	Δδ[a]	HL2	Pt-dppf-L2	HL3	Pt-dppf-L3	Δδ[a]	HL4	Pt-dppf-L4	Δδ[a]	HL5	Pt-dppf-L5	Δδ[a]
2	8.84 (dd)(1)	8.57 (d)(1)	-0.27	9.02 (dd)(1)	9.38 (d)(1)	9.00 (d)(1)	8.68 (d)(1)	-0.32	8.97 (dd)(1)	8.66 (d)(1)	-0.31	8.87 (dd)(1)	8.45 (d)(1)	-0.42
3	7.54 (dd)(1)	7.22 (m)(1)	-0.32	7.89 (dd)(1)	7.53 (dd)(1)	7.75 (dd)(1)	7.37 (dd)(1)	-0.38	7.77 (dd)(1)	7.35 (dd)(1)	-0.42	7.73 (dd)(1)	7.31 (dd)(1)	-0.42
4	8.31(dd)(1)	7.14 (d)(1)	-1.17	9.15 (dd)(1)	7.69 (m)(9)	8.50 (d)(1)	7.77 (s)(1)	-0.73	8.50(dd)(1)	7.62 (m)(1)[b]	-0.88	8.29 (dd)(1)	7.61 (m)(1)[b]	-0.68
5	7.38 (dd)(1)	7.64 (m)(1)[b]	0.26	-	-	-	-	-	-	-		-	-	-
6	7.44 (m)(1)	7.45 (m)(1)[b]	0.01	8.55(d)(1)	8.59 (d)(1)	7.82 (s)(1)	7.81 (m)(1)[b]	-0.01	8.00 (s)(1)	8.01 (s)(1)	0.01	8.34 (s)(1)	8.27 (s)(1)	-0.07
7	7.09 (dd)(1)	6.32 (d)(1)	-0.77	7.20 (d)(1)	6.25 (d)(1)	-	-	-	-	-		-	-	-
H_α	-	5.17 (s)(2)	1.24		5.24 (s)(2)		5.26 (s)(2)	1.33		5.05 (s)(2)	1.12		5.05 (s)(2)	1.12
		3.55 (s)(2)	-0.38	-	3.57 (s)(2)		3.47 (s)(2)	-0.46		3.66 (s)(2)	-0.27		3.66 (s)(2)	-0.27
H_β	-	4.81 (s)(2)	0.55	-	4.84 (s)(2)		4.82 (s)(2)	0.56		4.78 (s)(2)	0.52		4.78 (s)(2)	0.52
		4.52 (s)(2)	0.26		4.55 (s)(2)		4.52 (s)(2)	0.26		4.55 (s)(2)	0.29		4.55 (s)(2)	0.29

[a] $\Delta\delta$: $\delta_{complex}$-δ_{ligand}.
[b] Overlapped with PPh_2 protons signals.
Multiplicity: s: singlet, d: doublet, dd: doublet of doublets, t: triplet, m: multiplet.

~17 μM). Independently of the ligand, complexation to the {Pt-dppf} moiety increased 1.2- to 8-fold the cytotoxicity of the 8-hydroxyquinoline derivatives with respect to the free ligands.

Estimation of the selectivity index (SI = IC_{50} murine macrophage/ IC_{50} *T. brucei*) for each free HL compound showed values higher than 10 (SI of Nifurtimox) for HL2, HL4 and HL5. Ligand HL1 and dppf lacked specificity towards *T. brucei* (both SI < 4). Despite complexation of the ligands to {Pt-dppf} increased the cytotoxicity against macrophages, the selectivity indexes of the complexes were 2- to 9- fold higher than those of the corresponding ligands. The exception was Pt-dppf-L2, which showed a similar SI value than the free ligand HL2. Importantly, except for Pt-dppf-L1, all metal-based compounds have higher SI than Nifurtimox. The most potent and selective compound of the series is Pt-dppf-L4 (IC_{50} 0.14 μM, SI 48).

3.3.2. Cytotoxicity on A2780 and A2780cisR ovarian cells

The aim of this study was to determine the antiproliferative effect of the novel platinum complexes in two ovarian cancer cell lines, the cisplatin sensitive A2780 and the cisplatin resistant A2780cisR, and to compare with cisplatin. The compounds were also tested against a non-cancer cell line (V79) to determine the specificity of the compounds towards the cancer cells.

Independently of the type of cell line (A2780 or V79 cells) and with exception of HL2, the cytotoxicity of the ligands was *c.a.* one order of magnitude higher when coordinated to {Pt-dppf} (Table 5). In general, the cytotoxic activity of the complexes in both mammalian cell lines followed the same trend, *i.e.,* the coordination of the {Pt-dppf} *core* to the hydroxyquinoline derivatives increased the cytotoxicity (Table 4). Interestingly, the complexes with HL1, HL3-HL5 displayed IC_{50} values against A2780 cells one order of magnitude lower than that of the reference drug cisplatin (IC_{50} 26.0 ± 5.0 μM). Furthermore, comparison of the IC_{50} values obtained against the fibroblasts and the ovarian-cancer cells indicated that the free ligand HL1 (SI ~10) was selective towards the tumor cells, but none of the metal complexes presented considerable selectivity (SI < 3) (Table 5). It is also important to note that Pt-dppf-L2 showed low solubility in DMSO, which may affect the distribution of the compound in the cellular medium.

With the aim to investigate whether the new complexes could have the ability to overcome drug resistance, their antitumoral activity was evaluated against the A2780cisR cells, which display a 3-fold higher

Table 4
In vitro activity against the infective stage of *T. brucei* and J774 murine macrophages, selectivity index (SI) values and lipophilicity (R_f, R_M) of [Pt(L)(dppf)](PF_6) complexes, HL and dppf (included for comparison).

Compound	*T. brucei* IC_{50} ± SD (μM)	J774 IC_{50} ± SD (μM)	SI[a]	R_f[b]	R_M[b]
dppf	> 10	45 ± 6	< 4	ND	ND
HL1	12.4 ± 0.8	16.6 ± 1.5	1.3	0.73	−0.43
HL2	0.8 ± 0.3	31.1 ± 1.2	38.9	0.73	−0.43
HL3	2.5 ± 0.2	21.0 ± 0.8	8.4	0.31	0.35
HL4	2.4 ± 0.4	38.8 ± 6.7	16.2	0.23	0.51
HL5	3.0 ± 0.2	49.4 ± 9.1	16.4	0.19	0.65
Pt-dppf-L1	0.3 ± 0.1	3.4 ± 0.4	11.3	0.13	0.84
Pt-dppf-L2	0.93 ± 0.03	25.8 ± 1.5	27.7	0.10	0.97
Pt-dppf-L3	0.22 ± 0.01	3.4 ± 0.2	15.5	0.11	0.91
Pt-dppf-L4	0.14 ± 0.05	6.7 ± 0.4	47.8	0.08	1.04
Pt-dppf-L5	0.22 ± 0.04	6.4 ± 0.3	29.1	0.08	1.07
Nifurtimox	15 ± 3	150 ± 5[c]	10	ND	ND

ND: not determined.
[a] SI, selectivity index: (IC_{50} J774 murine macrophages/IC_{50} *T. brucei*).
[b] R_f and R_M values (lipophilicity) obtained using reverse phase TLC and MeOH: DMF:H_2O (65:5:30 v/v/v) as mobile phase.
[c] Data from [66].

Table 5
Cytotoxic activity (IC_{50}) of the ligands (HL1-HL5) and the corresponding [Pt(L)(dppf)](PF_6) compounds against A2780 cells after 24 h treatment. Results are expressed as mean ± SD of two independent experiments done with at least six replicates per condition.

Compound	IC_{50} (μM), 24 h	IC_{50} (μM), 24 h	SI
	A2780	V79	
HL1	11.0 ± 3.6	104 ± 32	9.5
HL2	20.4 ± 6.0	20.4 ± 5.0	1.0
HL3	12.4 ± 3.5	42.6 ± 22	3.4
HL4	33.4 ± 6.9	59.0 ± 15	1.7
HL5	41.1 ± 9.6	60.1 ± 13	1.5
Pt-dppf-L1	4.4 ± 1.5	1.7 ± 0.3	0.4
Pt-dppf-L2	52.2 ± 15	58.4 ± 24	1.1
Pt-dppf-L3	2.7 ± 0.8	2.1 ± 0.4	0.8
Pt-dppf-L4	1.3 ± 0.4	3.1 ± 0.2	2.3
Pt-dppf-L5	1.2 ± 0.1	4.0 ± 1.7	3.4
Cisplatin	26.0 ± 5.0	–	–

SI: IC_{50} V79/IC_{50}A2780.

Table 6
Cytotoxic activity (IC_{50}) of the new Pt compounds in the A2780cisR after 24 h treatment. Results are mean ± SD of two independent experiments done with at least six replicates per condition.

Compound	IC_{50} (μM)
Pt-dppf-L1	11.5 ± 6.0
Pt-dppf-L2	> 100
Pt-dppf-L3	16.7 ± 6.3
Pt-dppf-L4	1.5 ± 0.55
Pt-dppf-L5	3.0 ± 1.2
Cisplatin	75.4 ± 20

resistance against cisplatin than the parental cell line A2780 (Tables 5 and 6). Unlike cisplatin and with the exception of L2 and L3 complexes, the complexes in the A2780 resistant cells displayed IC_{50} values in the same order of magnitude than those found for the parental A2780 cells (Table 6). These results suggest that these compounds exert their cytotoxic effect towards tumor cells *via* mechanisms that overcome cisplatin resistance. The data also highlight the effect of the substituent nature on the quinoline framework on the antitumoral activity.

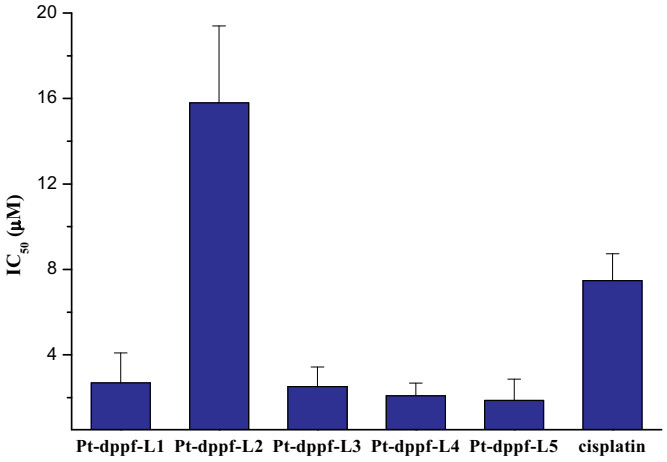

Fig. 3. Cytotoxic activity (IC_{50}) of the complexes [Pt(L)(dppf)](PF_6) and the reference drug cisplatin in the A2780 cells after 48 h treatment. Results are mean ± SD of two independent experiments done with at least six replicates per condition.

At 24 h incubation the most active compounds of the series were Pt-dppf-L4 (IC_{50} 1.3 μM) and Pt-dppf-L5 (IC_{50} 1.2 μM) with one and two iodine substituents, respectively.

Considering that 24 h incubation could be a short time for testing cisplatin or even some of the Pt complexes, the MTT assay was also performed after 48 h incubation. Results depicted in Fig. 3 show that Pt-dppf-L2, the less cytotoxic compound of the series, and cisplatin, both benefit from longer incubation time. However, no improvement of the cytotoxic activity was shown by the other Pt complexes.

3.4. Lipophilicity

Given the importance of this physicochemical property in the transmembrane transport and interaction with biological receptors, it is important to determine if there is a correlation between lipophilicity and the observed biological activity of a prospective drug [67]. The effect of complexation of the 8-hydroxyquinoline derivatives on lipophilicity was experimentally determined using reversed-phase TLC, where the stationary phase (precoated TLC-C18) may be considered to simulate lipids of biological membranes or receptors, and the mobile phase (MeOH: DMF: H_2O (65:5:30 v/v/v)) may be considered as the aqueous biological milieu. The composition of the mobile phase was tuned-up in order to allow to differentiate complexes and free ligands according to their lipophilicity. Results of measured R_f and resulting R_M value are shown in Table 4. As expected, the lipophilicity increased from the free ligand to its corresponding Pt-dppf compound due to the inclusion of the {Pt-dppf} moiety (higher the R_M value, higher the lipophilicity).

When comparing the biological activity of the compounds with their lipophilicity, a possible correlation was found. Considering Pt-dppf-L2 compound as an outlier due to its single poliatomic substituent in the position 5 of the quinolinic ring, the rest of the series showed a nearly parabolic correlation between R_M (lipophilicity) and the anti-*T. brucei* activity (IC_{50} values) (Fig. S3). The minimum of this parabola corresponded to Pt-dppf-L4, which is also the most active and the most selective compound of the series towards *T. brucei*. While the number of structurally related compounds in this case is too low to establish clear correlations, a more in-depth Quantitative structure–activity relationship (QSAR) study including the whole series of related {M(dppf)} compounds developed by us that also considers other properties, is currently being carried out [25–27].

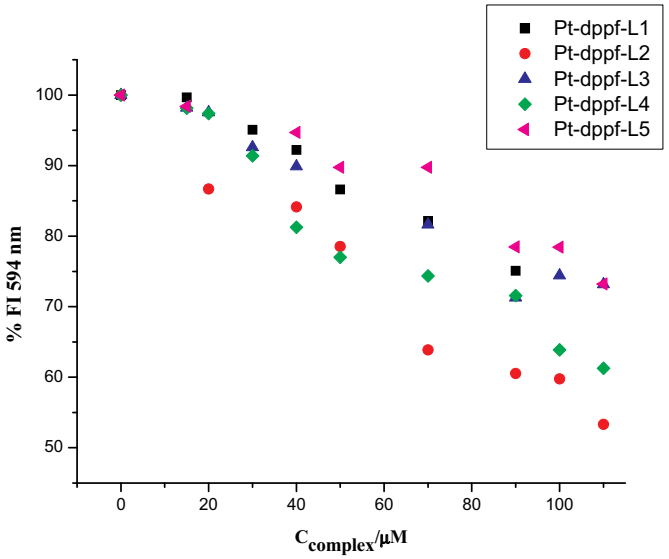

Fig. 4. Titration of {DNA-Ethidium bromide} adduct with Pt-dppf-L complexes. Relative fluorescence intensity (%) at λ_{em} = 594 nm of the {DNA-EB} adduct (C_{DNA} = 20 μM, C_{EB} = 10 μM, samples prepared in 5% DMSO/Tris HCl medium) with increasing concentration of the five metal complexes upon 30 min incubation at 37 °C. Squares: Pt-dppf-L1; circles: Pt-dppf-L2; up triangles: Pt-dppf-L3; diamonds: Pt-dppf-L4; left triangles: Pt-dppf-L5.

3.5. Insight into the mechanism of action

3.5.1. DNA interaction

Ethidium bromide (EB) was employed to study the interaction of the new complexes with DNA. EB is a planar molecule with weak intrinsic fluorescence emission at the selected excitation wavelength of 510 nm. Under the selected experimental conditions EB shows an emission maximum at 601 nm. Intercalation of the dye into double stranded DNA induces a high increase of the fluorescence quantum yield [68]. Additionally, in the experimental conditions the emission maximum of the {DNA-EB} adduct is located at 594 nm. At the selected excitation wavelength DNA, HL1-HL5 ligands and Pt-dppf complexes are non-fluorescent at pH = 7.4 10 mM Tris/5% DMSO, and no fluorescence emission results from the direct interaction of the complexes or the ligands with DNA. The complexes showed negligible absorption at 594 nm in the concentration range used. Results obtained for the titration of the {DNA-EB} adduct with the new compounds are depicted in Fig. 4. When the concentration of the Pt-dppf complexes is increased, a quenching in the emission of {DNA-EB} adduct is observed. The extent of the quenching is of similar order for the five complexes. These results are consistent with an interaction of the compounds with the DNA that induces conformational changes and displaces EB from the {DNA-EB} complex, in the conditions tested. The technique does not allow determining the kind of interaction established.

The mechanisms involved in the fluorescence quenching process for the complexes can be accessed by a Stern-Volmer analysis according to

$$\frac{IF_0}{IF} = 1 + K_{SV}[Q] \quad (1)$$

where IF_0 and IF is the emission fluorescence intensity of the {DNA-EB} adduct in the absence and in the presence of the complex, K_{SV} the Stern-Volmer constant, and [Q] the concentration of the quencher (in this case, the complexes) [69]. Eq. (1) predicts a linear plot for IF_0/IF for a homogeneously emitting system. Stern-Volmer analysis showed a linear IF_0/IF plot (Fig. 5) and the K_{SV} constant can be calculated for each system (Table 7). Although K_{SV} informs about the quenching produced by the compounds, it is an useful parameter that indirectly indicates the affinity of the compounds for the DNA.

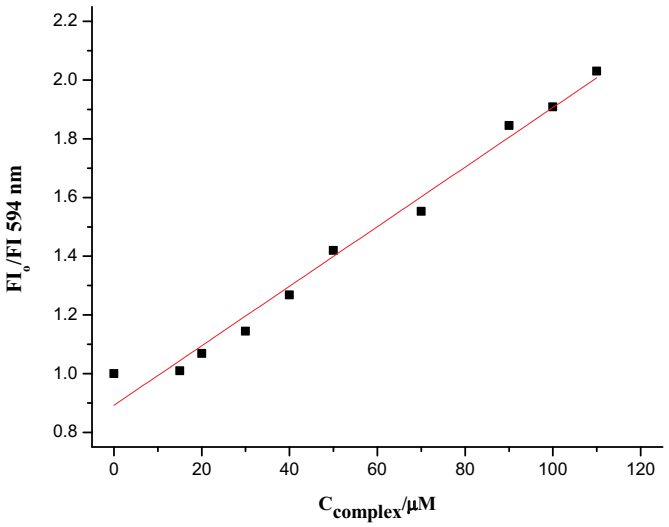

Fig. 5. Stern-Volmer plot for Pt-dppf-L1.

Table 7
Stern-Volmer constants of the Pt-dppf complexes for the competitive binding to {DNA-EB} adduct in 5% DMSO/Tris HCl medium.

Compound	K_{SV} (M^{-1})	Log (K_{SV})
Pt-dppf-L1	2102	3.3
Pt-dppf-L2	7744	3.9
Pt-dppf-L3	3599	3.6
Pt-dppf-L4	6053	3.8
Pt-dppf-L5	3505	3.5

Results depicted in Table 7 show that all complexes tested interact with DNA independently of the nature of the 8-hydroxyquinoline derivative. Obtained *K*sv values for the five complexes are of similar order to those previously reported by us for other complexes showing antitrypanosomal activity [26,70]. The *K*sv values obtained were lower than those previously reported for other complexes with typical planar DNA intercalating ligands [71].

It is noteworthy to mention that none of the free ligands affect the emission of the {DNA-EB} adduct, except for HL2 that generates a slight decrease of fluorescence (data not shown). Nevertheless, the K_{SV} value found for its Pt-dppf-L2 complex was higher than that found for the free ligand (log K_{SV} = 3.0). These results show that in every case the coordination of the HL ligand to the {Pt-dppf} moiety generates an interaction between the obtained complexes and the {DNA-EB} adduct, which was absent in the case of the free ligands. The whole set of results suggests that DNA could be a molecular target of these complexes.

3.5.2. Intracelullar ROS levels in A2780 cells

Cisplatin and most of the anticancer drugs induce the formation of ROS. The anticancer effect is thought to be mediated by the increase of oxidative stress that by its turn can activate cell death mechanisms and induce apoptosis [72]. Dihydrofluorescein diacetate is a widespread probe for ROS detection based on the oxidation of the cell permeant non-fluorescent reagent (H_2DCFDA) to yield the highly fluorescent dichlorofluorescein (DCF) by intracellular esterases. This method is known for its high sensibility to detect ROS production particularly hydrogen peroxide and hydroxyl radical in intact cells [73]. As ROS are chemically reactive molecules, complexes were assayed at shorter incubation times. The concentrations used in the assays were selected taking into consideration the IC_{50} values of the complexes at 3 h incubation (Table 8).

The induction of intracellular ROS by the five [Pt(L)(dppf)](PF_6) compounds in the A2780 cells was analyzed at $\lambda_{exc.}$ = 492 nm and

Table 8
Cytotoxic activity (IC_{50}) of complexes in the A2780 cells after 3 h treatment. Results are mean ± SD of two independent experiments done with at least six replicates per condition.

Compound	IC_{50} (μM)
Pt-dppf-L1	10.8 ± 3.6
Pt-dppf-L2	> 100
Pt-dppf-L3	21.7 ± 2.0
Pt-dppf-L4	10.7 ± 2.2
Pt-dppf-L5	7.4 ± 1.3

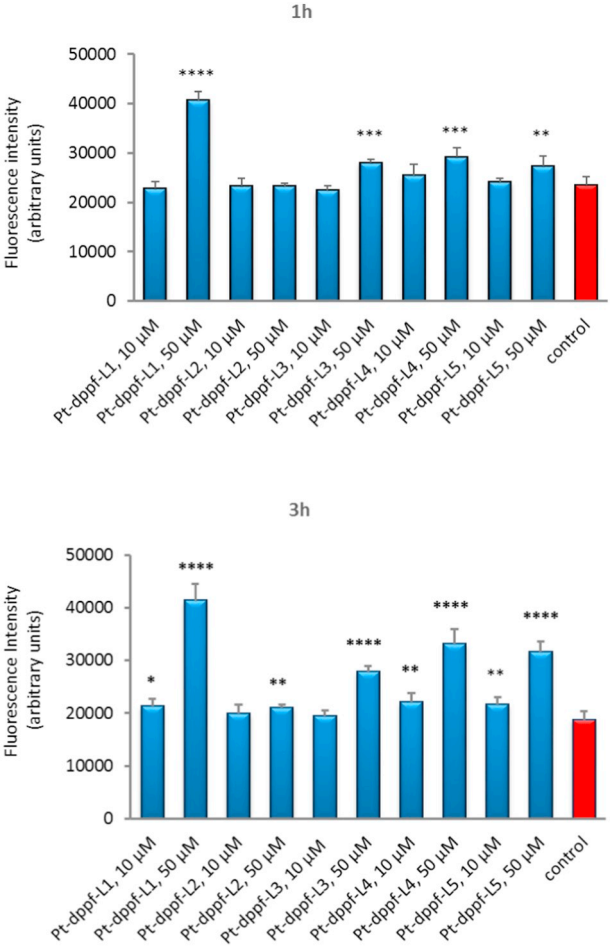

Fig. 6. Reactive oxygen species (ROS) induced by the complexes Pt-dppf-L with HL = HL1-HL5, using the fluorescent probe H_2DCFDA. With the exception of Pt-dppf-L2, all the complexes induce ROS formation, in particular Pt-dppf-L1. This effect was more evident by increasing the incubation time from 1 h to 3 h. Results are mean ± SD of a typical experiment done with at least six replicates per condition. $*p \leq 0.05$; $**p \leq 0.01$; $***p \leq 0.001$; $****p \leq 0.0001$. The control means cells with no treatment.

$\lambda_{em.}$ = 517 nm. As shown in Fig. 6, and with the exception of the less active compound [Pt(L2)(dppf)](PF_6), all the complexes induce ROS formation, in particular [Pt(L1)(dppf)](PF_6). This effect was more evident increasing the incubation time. At 10 and 50 μM, incubation for additional 2 h led to a higher increase in ROS levels for the complexes with HL = HL3, HL4 and HL5, whereas for HL1 ROS production retained the level achieved upon 1 h treatment. These results indicate that the cytotoxic effect of the Pt complexes may, in part, be mediated by ROS. In fact, the high concentrations of compounds required to put in evidence the formation of ROS along with the normo-sensitivity displayed by the cisplatin-resistant cells towards most of these compounds suggest that other mechanisms of action may be involved in addition to the resulting intracellular redox unbalance. The chemotherapeutic drugs cisplatin and doxorubicin were also included in the study as positive controls, to confirm their ability to induce ROS formation in the test conditions (Fig. S4).

Table 9
Pt uptake by A2780 cells exposed to the complexes. The content of Pt was determined by ICP-MS in cell pellets. The uncertainty for the Pt determination is included.

Compound	Pt (pg/10^6 cells)
Pt-dppf-L1	11.9 ± 0.6
Pt-dppf-L2	200 ± 10
Pt-dppf-L3	12.6 ± 0.6
Pt-dppf-L4	10.5 ± 0.5
Pt-dppf-L5	10.9 ± 0.5
Control (cells only)	< 0.05[a]

[a] Value 100 times below calibration range limit.

3.6. Pt cellular uptake by ICP-MS

These studies were carried out to evaluate any relationship between the total Pt uptake by the A2780 cells and the nature of the substituent on the quinoline framework of the complexes upon 3 h incubation at a concentration equivalent to their IC_{50} values (Table 8). All cells showed significant uptake of Pt compared to control (no treated cells) where the Pt level was virtually nil (Table 9). The most striking result was the increased uptake of cells treated with Pt-dppf-L2, where the content of Pt was 15–20 folds higher than for the other complexes tested. In the cell studies Pt-dppf-L2 was the less active complex of the series probably due to its low solubility in the cellular medium and/or its inactivation inside the cells, no matter the higher uptake. For the other complexes of the series the cellular uptake was virtually the same. Results pointed to the fact that not always the cellular uptake can be correlated with the cytotoxic activity.

4. Conclusions

A series of five new [Pt(L)(dppf)](PF_6) compounds, with HL = 8-hydroxyquinoline derivatives and dppf = 1,1′-bis(dipheny1phosphino) ferrocene, was synthesized and fully characterized in the solid state and in solution. These new Pt^{II}-compounds showed good activity against bloodstream *T. brucei* and good selectivity towards the pathogen, far superior than those for the reference drug Nifurtimox. With the exception of HL2 complex, the new {Pt-dppf} compounds showed an improvement in activity and in selectivity towards the parasite with respect to free ligands and the dppf co-ligand. The most potent and selective compound of the series was [Pt^{II}(L4)(dppf)](PF_6) (IC_{50} 0.14 μM, SI 48), being the most promising compound for further anti-*T. brucei* drug developments.

Compounds were also evaluated for their cytotoxicity in A2780/A2780cisR ovarian cells. With the exception of Pt-dppf-L2, all complexes displayed cytotoxic activity superior than the reference platinum drug cisplatin at several time points. As for the parasites the nature of the substituents in the quinoline moiety had an effect on the cytotoxicity. This effect could be related with the different electron donating or accepting properties of the selected substituents. The iodine substituents proved to increase the activity. The compounds showed IC_{50} values against A2780cisR cells of the same order of magnitude than those found for the A2780 cells.

In what respects the mechanism of cell death, the compounds induced the formation of ROS with exception of the less active compound Pt-dppf-L2. The interaction of the complexes with DNA suggested that this biomolecule could be a potential target either in the parasites or in the tumor cells.

No correlation between cytotoxicity and cellular uptake could be established. Lipophicility showed a nearly parabolic correlation with the anti-*T. brucei* activity (IC_{50} values) of the compounds, being needed further QSAR studies, including the whole series of related {M-dppf} compounds developed by us, to assess a clear correlation of lipophilicity and other properties with the antitrypanosomal activity.

To sum up, results indicate that the compounds presented herein could be interesting to be further explored as new agents to aid in parasitic diseases and cancer treatment and to contribute to the understanding of the similarities between this type of highly proliferating cells.

Acknowledgements

F.R. and E.R.A. acknowledge the support of the Agencia Nacional de Investigación e Innovación (ANII, Uruguay) through the grants POS_NAC_2016_1_129899 and POS_NAC_2018_1_151206 and POS_NAC_2015_1_110215, respectively. This work was supported by PEDECIBA Uruguay. M.A.C. acknowledges the support of ANII (grant PR_FMV_2009_1_2617) and FOCEM (MERCOSUR Structural Convergence Fund, COF 03/11). F.M. and T.P. acknowledge the support of the Fundação para a Ciência e a Tecnologia (contracts UID/MULTI/04349/2013 and UID/BIO/04565/2013) and LISBOA-01-0145-FEDER-007317. Authors thank F. Araújo for allocation of equipment time at the HPLC/ICP-MS Laboratory of C2TN/IST, and S.S. Gomes for the assistance with ICP-MS operation.

Appendix A. Supplementary data

Supplementary data to this article can be found online at https://doi.org/10.1016/j.jinorgbio.2019.110779.

References

[1] http://www.who.int/trypanosomiasis_african/ (visited 2019).
[2] M. Berninger, I. Schmidt, A. Ponte-Sucre, U. Holzgrabe, MedChemComm 8 (2017) 1872–1890.
[3] V. Delespaux, H.P. de Koning, Drug Resist. Updat. 10 (2007) 30–50.
[4] https://www.who.int/cancer/en/.
[5] B. Oronsky, C.M. Ray, A.L. Spira, J.B. Trepel, C.A. Carter, H.M. Cottrill, Med. Oncol. 34 (2017) 103.
[6] K.J. Franz, N. Metzler-Nolte, Chem. Rev. 119 (2019) 727–729.
[7] M. Navarro, G. Gabbiani, L. Messori, D. Gambino, Drug Discov. Today 15 (2010) 1070–1077.
[8] R.A. Sánchez-Delgado, A. Anzellotti, Mini-Rev. Med. Chem. 4 (2004) 22–30.
[9] D. Gambino, L. Otero, Inorg. Chim. Acta 472 (2018) 58–75.
[10] D. Gambino, Coord. Chem. Rev. 255 (2011) 2193–2203.
[11] J. Costa Pessoa, S. Etcheverry, D. Gambino, Coord. Chem. Rev. 301–302 (2015) 24–48.
[12] Y. Ching Ong, S. Roy, P.C. Andrews, G. Gasser, Chem. Rev. 119 (2019) 730–796.
[13] R.W. Brown, C.J.T. Hyland, Med. Chem. Commun. 6 (2015) 1230–1243.
[14] M.B. Camarada, C. Echeverria, R. Ramirez-Tagle, Med. Chem. Commun. 7 (2016) 1307–1315.
[15] A. Tahghighi, J. Organomet. Chem. 770 (2014) 51–60.
[16] R.H. Fish, G. Jaouen, Organometallics 22 (2003) 2166–2177.
[17] C. Biot, Curr. Med. Chem. - Anti-Infective Agents 3 (2004) 135–147.
[18] C. Biot, D. Dive, Top. Organomet. Chem. 32 (2010) 155–193.
[19] D.R. van Staveren, N. Metzler-Nolte, Chem. Rev. 104 (2004) 5931–5985.
[20] B.P.S. Milena, J.F.O. Costa, M.S. de Sá, R. Ribeiro-dos-Santos, P. Pigeon, G. Jaouen, A.E.G. Santana, M.O.F. Goulart, E. Hillard, Drug Dev. Res. 71 (2010) 69–75.
[21] S. Pomel, F. Dubar, D. Forge, P.M. Loiseau, C. Biot, Bioorg. Med. Chem. 23 (2015) 5168–5517.
[22] J. Gómez, A.H. Klahn, M. Fuentealba, D. Sierra, C. Olea-Azar, J.D. Maya, M.E. Medina, J. Organomet. Chem. 839 (2017) 108–115.
[23] K. Kinnamon, E.A. Steck, E.S. Rane, Antimicrob. Agents Chemother. 15 (1979) 157–160.
[24] Z. Lun, D. Lai, Y. Wen, L. Zheng, J. Shen, T. Yang, W. Zhou, L. Qu, G. Hide, F.J. Ayala, Proc. Natl. Acad. Sci. U. S. A. 112 (2015) 8835–8842.
[25] E. Rodríguez Arce, M.F. Mosquillo, L. Pérez-Díaz, G.A. Echeverría, O.E. Piro, A. Merlino, L. Coitiño, C. Maríngolo Ribeiro, C.Q.F. Leite, F.R. Pavan, L. Otero, D. Gambino, Dalton Trans. 44 (2015) 14453–14464.
[26] F. Rivas, A. Medeiros, E. Rodríguez Arce, M. Comini, C.M. Ribeiro, F.R. Pavan, D. Gambino, J. Inorg. Biochem. 187 (2018) 73–84.
[27] E. Rodríguez Arce, E. Putzu, M. Lapier, J.D. Maya, C. Olea Azar, G.A. Echeverría, O.E. Piro, A. Medeiros, F. Sardi, M. Comini, G. Risi, G. Salinas, I. Correia, J. Costa Pessoa, L. Otero, D. Gambino, Dalton Trans. 49 (2019) 7644–7658.
[28] M.F. Mosquillo, L. Bilbao, F. Hernández, I. Machado, D. Gambino, B. Garat, L. Pérez-Díaz, Biometals 31 (2018) 961–974, https://doi.org/10.1007/s10534-018-0140-4.
[29] M.F. Mosquillo, L. Bilbao, F. Hernández, F. Tissot, D. Gambino, B. Garat, L. Pérez-Díaz, Chem. Biol. Drug Design 92 (2018) 1657–1669.
[30] K. Nomiya, A. Yoshizawa, K. Tsukagoshi, N. Chikaraishi Kasuga, S. Hirakawa, J. Watanabe, J. Inorg. Biochem. 98 (2004) 46–60.
[31] T.A.K. Al-Allaf, H. Schmidt, K. Merzweiler, C. Wagner, D. Steinborn, J. Organomet. Chem. 678 (2003) 48–55.
[32] W.J. Geary, Coord. Chem. Rev. 7 (1971) 81–122.
[33] L. Krause, R. Herbst-Irmer, G.M. Sheldrick, D. Stalke, J. Appl. Crystallogr. 48 (2015) 3–10.
[34] G.M. Sheldrick, Acta Cryst. A 71 (2015) 3–8.
[35] O.V. Dolomanov, L.J. Bourhis, R.J. Gildea, J.A.K. Howard, H. Puschmann, J. Appl. Crystallogr. 42 (2009) 339–341.
[36] C.B. Hübschle, G.M. Sheldrick, B. Dittrich, J. Appl. Crystallogr. 44 (2011) 1281–1284.
[37] L. Szilágyi, K.E. Kövér, K. Fehér, M.A. Comini, Int. J. Parasitol. Drugs Drug Resist. 7 (2017) 303–313.
[38] F. Maiwald, D. Benítez, D. Charquero, M.A. Dar, H. Erdmann, L. Preu, O. Koch, C. Hölscher, N. Loaëc, L. Meijer, M.A. Comini, C. Kunick, Eur. J. Med. Chem. 18 (2014) 274–283.
[39] B. Demoro, C. Sarniguet, R. Sánchez-Delgado, M. Rossi, D. Liebowitz, F. Caruso, C. Olea-Azar, V. Moreno, A. Medeiros, M.A. Comini, L. Otero, D. Gambino, Dalton Trans. 41 (2012) 1534–1543.
[40] C. Hansch, A. Leo, The hydrophobic parameter: measurement and calculation, Exploring QSAR. Fundamentals and Applications in Chemistry and Biology, American Chemical Society Ed, Washington, 1995, pp. 97–124.
[41] H. Cerecetto, R. Di Maio, M. González, M. Risso, P. Saenz, G. Seoane, A. Denicola, G. Peluffo, C. Quijano, C. Olea-Azar, J. Med. Chem. 42 (1999) 1941–1950.
[42] J.K. Barton, J.M. Goldberg, Ch.V. Kumar, N.J. Turro, J. Am. Chem. Soc. 108 (1986) 2081–2088.
[43] M.A. Barreiros, T. Pinheiro, P.M. Félix, C. Franco, M. Santos, F. Araujo, M.C. Freitas, S.M. Almeida, J. Radioanal. Nucl. Chem. 297 (2013) 377–382.
[44] P.M. Félix, S.M. Almeida, T. Pinheiro, J. Sousa, C. Franco, H.T. Wolterbeek, Assessment of exposure to metals in lead processing industries, Int. J. Hyg. Environ. Health 216 (2013) 17–24.
[45] M.E. Mahmoud, S.S. Haggag, T.M. Abdel-Fattah, Polyhedron 28 (2009) 181–187.
[46] H.F. Aly, F.M. Abdel Kerim, A.T. Kandil, J. Inorg. Nucl. Chem. 33 (1971) 4340–4344.
[47] A. Sharma, D. Singh, J.K. Makrandi, M.N. Kamalasanan, R. Shrivastva, I. Singh, Mater. Lett. 61 (2007) 4614–4617.
[48] Z.F. Chen, Y.Q. Gu, X.Y. Song, Y.C. Liu, Y. Peng, H. Liang, Eur. J. Med. Chem. 59 (2013) 194–202.
[49] S.M. El-Megharbel, M.S. Refat, J. Mol. Struct. 1085 (2015) 222–234.
[50] Y.M. Hu, J. Qu, Y.L. Yi, H.L. Gao, J.Z. Cui, J. Coord. Chem. 66 (2013) 18–27.
[51] T. Hayashi, M. Konishi, Y. Kobori, M. Kumada, T. Higuchi, K. Hirotsu, J. Am. Chem. Soc. 106 (1984) 158–163.
[52] K.S.O. Ferraz, D.C. Reis, J.G. Da Silva, E.M. Souza-Fagundes, E.J. Baran, H. Beraldo, Polyhedron 63 (2013) 28–35.
[53] I. Potočňák, P. Vranec, Monatsh Chem 143 (2012) 217–226.
[54] A.C. González-Baró, E.J. Baran, Monatsh Chem 128 (1997) 323–335.
[55] C.C. Wagner, A.C. González-Baró, E.J. Baran, Spectrochim. Acta A 79 (2011) 1762–1765.
[56] A.M. Heyns, Spectrochim. Acta Part A: Molecular Spectroscopy 33 (1977) 315–322.
[57] J. Kljun, I.E. León, Peršič, J.F. Cadavid-Vargas, S.B. Etcheverry, W. He, Y. Bai, I. Turel, J. Inorg. Biochem. 186 (2018) 187–196.
[58] T. Ghosh, S. Bhattacharya, A. Das, G. Mukherjee, M.G.B. Drew, Inorg. Chim. Acta 358 (2005) 989–996.
[59] C. Martín Santos, S. Cabrera, C. Ríos-Luci, J.M. Padrón, I. López Solera, A.G. Quiroga, M.A. Medrano, C. Navarro-Ranninger, J. Alemán, Dalton Trans. 42 (2013) 13343–13348.
[60] O. Sigouin, A.L. Beauchamp, Can. J. Chem. 83 (2005) 460–470.
[61] B.C. Baker, D.T. Sawyer, Anal. Chem. 40 (1968) 1945–1951.
[62] S. Shahraki, A. Heidari, H.R. Mirzaei, M. Saeidifar, N. Ahmadinasab, H. Mansouri-Torshizi, J. Iran. Chem. Soc. 15 (2018) 697–709.
[63] A. Togni, T. Hayashi, Ferrocenes: Homogeneous Catalysis, Organic Synthesis, Materials Science, Weinheim - New York Basel - Cambridge. Tokyo (1995), pp. 41–43.
[64] C.E. Housecraft, S.M. Owen, P.R. Raithby, B.A.M. Shaykh, Organometallics 9 (1990) 1617–1623.
[65] D. Cauzzi, C. Graiff, C. Massera, G. Predieri, A. Tiripicchio, D. Acquotti, J. Chem. Soc. Dalton Trans. (1999) 3515–3521.
[66] D. Benítez, A. Medeiros, L. Fiestas, E.A. Panozzo-Zenere, F. Maiwald, K.C. Prousis, M. Roussaki, T. Calogeropoulou, A. Detsi, T. Jaeger, J. Šarlauskas, L.P. Mašič, C. Kunick, G.R. Labadie, L. Flohé, M.A. Comini, PLoS Negl. Trop. Dis. 10 (2016) e0004617.
[67] E.H. Kerns, L. Di, Drug-Like Properties: Concepts, Structure Design and Methods From ADME to Toxicity Optimization, Academic Press, Amsterdam, 2008.
[68] J.B. Lepecq, C. Paoletti, J. Mol. Biol. 27 (1967) 87–106.
[69] J.R. Lakowicz, Principles of Fluorescence Spectroscopy, 3rd. ed., Springer Science, New York, 2006 (Chapter 8).
[70] M. Fernández, E.R. Arce, C. Sarniguet, T.S. Morais, A.I. Tomaz, C.O. Azar, R. Figueroa, J. Diego Maya, A. Medeiros, M. Comini, M. Helena Garcia, L. Otero, D. Gambino, J. Inorg. Biochem. 153 (2015) 306–314.
[71] B.Y. Wu, L.H. Gao, Z.M. Duan, K.Z. Wang, J. Inorg. Biochem. 99 (2005) 1685–1691.
[72] H. Yang, R. Villani, H. Wang, M.J. Simpson, M.S. Roberts, M. Tang, X. Liang, J. Exp. Clin. Cancer Res. 37 (2018) 266.
[73] X. Wang, H. Fang, Z. Huang, W. Shang, T. Hou, A. Cheng, H. Cheng, J. Mol. Med. (Berl). 91 (2013) 917–927.